PERGAMON

International Journal of Heat and Mass Transfer 43 (2000) 1173–1185

International Journal of HEAT and MASS TRANSFER

www.elsevier.com/locate/ijhmt

Suspension-to-membrane-wall heat transfer in a circulating fluidized bed combustor

W. Luan [1], B.D. Bowen, C.J. Lim, C.M.H. Brereton, J.R. Grace*

Department of Chemical and Bio-Resource Engineering, University of British Columbia, Vancouver, Canada V6T 1Z4

Received 4 May 1998; received in revised form 2 June 1999

Abstract

Suspension-to-membrane-wall heat transfer was studied in a pilot scale circulating fluidized bed combustor at 700 and 800°C for suspension densities of 10–70 kg/m^3 with 286 μm silica sand particles. The total suspension-to-membrane-wall heat transfer coefficient is determined using the exposed-pipe-radial, insulated-pipe-tangential, fin-one-dimensional heat transfer model of Bowen et al. [B.D. Bowen, M. Fournier, J.R. Grace, Heat transfer in membrane waterwalls, Int. J. Heat Mass Transfer 34 (1991) 1043–1057]. Suspension-to-pipe and suspension-to-fin transfer is also determined from temperatures measured by embedded thermocouples. The fin accounted for about one third of the total heat transfer, and most of this portion passed through the insulated portion of the pipe.

Keywords: Fluidization; Heat transfer; Radiation; Circulating fluidized bed; Membrane wall; Gas–solid suspension

1. Introduction

Information on heat transfer in circulating fluidized beds at high temperatures using membrane walls as heat transfer surfaces is scarce. Membrane walls commonly used in industrial boilers are of two types, the 'American type' where the fin is welded to the pipe, and the 'Walther type' where the fin is an integral part of the pipe [1].

Heat transfer coefficients near the crest and in the valleys between adjacent pipes can be quite different. Lockhart et al. [2] carried out cold model experiments in a circular riser with a simulated membrane wall consisting of two groups of pipes of different diameter (19 and 32 mm), for three suspension densities at a superficial gas velocity of 7 m/s. The heat transfer coefficients were found to increase with particle concentration and to be higher along the fin than on the crest. Wu et al. [3] tested an 'American type' membrane wall at high temperatures. Their data show that the total coefficients obtained with a membrane wall are lower than those obtained with a vertical pipe within the suspension close to a flat wall. Andersson and Leckner [1] embedded 10 thermocouples in a pipe and its adjacent fin to examine the temperature differences between the crests and valleys of a 'Walther type' membrane wall. There was a maximum variation of only 6–10°C between thermocouples, a small difference compared to the temperature difference between the pipe and the particles. They also measured suspension-to-fin heat fluxes and found lower heat transfer coefficients in the fin area, where the particle concentration is higher than in the crest region. The expla-

* Corresponding author. Tel.: +1-604-822-3121; fax: +1-604-822-6003.

E-mail address: jgrace@chml.ubc.ca (J.R. Grace).

[1] Present address. USG Corporation, Libertyville, IL 60048-1296, USA.

0017-9310/00/$ - see front matter
PII: S0017-9310(99)00198-2

Nomenclature

A	exposed area (m^2)
Bi	Biot number, $Bi = hR/k_p$
c_p	specific heat (W kg^{-1} K^{-1})
d_p	particle diameter (μm)
H	height of riser (m)
h	heat transfer coefficient (W m^{-2} K^{-1})
k	thermal conductivity (W m^{-1} K^{-1})
L	length of membrane wall (m)
M_{cw}	mass flow rate of cooling water (kg s^{-1})
P/S	ratio of primary air flow to secondary air flow
Q	heat transfer rate (W)
Q_{ins}	heat transfer rate through insulated portion of pipe (W)
R	radius of membrane pipe (m)
r	coordinate in cylindrical coordinates, or radius (m)
T	temperature (K or °C)
$T_1,\ldots,T_6$	pipe and fin temperatures measured by embedded thermocouples (see Fig. 1) (K or °C)
T_{ave}	temperature at center of pipe wall adjacent to fin (see Fig. 4) (K or °C)
T_b	bulk suspension temperature (K or °C)
T_{surf}	weighted average exposed surface temperature of pipe and fin (K or °C)
T_t	outside surface temperature of membrane pipe (K or °C)
T_w	water temperature (K or °C)
U_g	superficial gas velocity (m s^{-1})
w	half-width of fin (m)
x	distance from fin (m)
z	height from gas distributor to location of thermocouple in pipe (m)

Greek symbols

α	dimensionless inside radius of pipe, $\alpha = R_i/R_o$
β	dimensionless fin half-thickness, $\beta = \delta_f/R_o$
γ	dimensionless fin width, $\gamma = w/R_o$
δ_f	half-thickness of fin (m)
ζ	dimensionless fin conductivity, $\zeta = k_f/k_p$
ρ_{susp}	suspension density (kg m^{-3})
ϕ	angle subtended by base of fin (see Fig. 4) (rad)
ω	angle subtended by insulated or exposed portion of half-pipe (see Fig. 4) (rad)

Subscripts

cw	cooling water
f	fin
g	gas
i	inside
in	inlet to membrane assembly
m	measured
o	outside
out	outlet of membrane assembly
p	pipe
t	total

nation is that denser shielded suspension descending along the fin equilibrate with the surface so that radiative and convective heat transfer decrease as particles near the wall are cooled [4,5].

2. Experimental details

Our experiments were carried out in a pilot scale CFB combustion facility where the riser has a 152 mm square cross-section and a 7.3 m overall height (see Ref. [3] for more details). For the tests described in this paper, bulk temperatures between about 800 and 900°C were achieved by burning Pennsylvania coal with approximately 15% excess air.

The heat flux from a suspension to a membrane wall can be calculated using temperatures measured by thermocouples embedded in the pipes and fins [1,6,7–9]. In this study, temperature profiles close to the pipe crest and suspension-to-pipe and suspension-to-fin heat fluxes were measured by embedded thermocouples. Experiments were carried out using the membrane wall heat transfer surface [10], shown schematically in Fig. 1, consisting of four identical pipes (21.3 mm O.D. and 14.1 mm I.D.) and connecting fins (12.7 mm in width). The total length of the membrane section was 1.626 m, and its top was 1.321 m below the top of the riser. The tube and fin involved in the measurements reported in this paper were made of stainless steel 316. The emissivity of the stainless steel assembly after exposure to the combustion conditions is estimated to have been 0.50 [11]. The solids were Ottawa silica sand particles of mean diameter 286 μm whose relevant properties are listed in Table 1.

Eight K-type thermocouples were installed at the centerline of one of the pipes to measure water temperatures at different elevations, including the water inlet and water outlet (see Fig. 1). To measure the temperature profile within the wall and fin of that pipe 5.44 m above the primary air distribution, six 0.508 mm diameter K-type thermocouples were embedded in one SS316 pipe wall and adjacent fin as indicated by

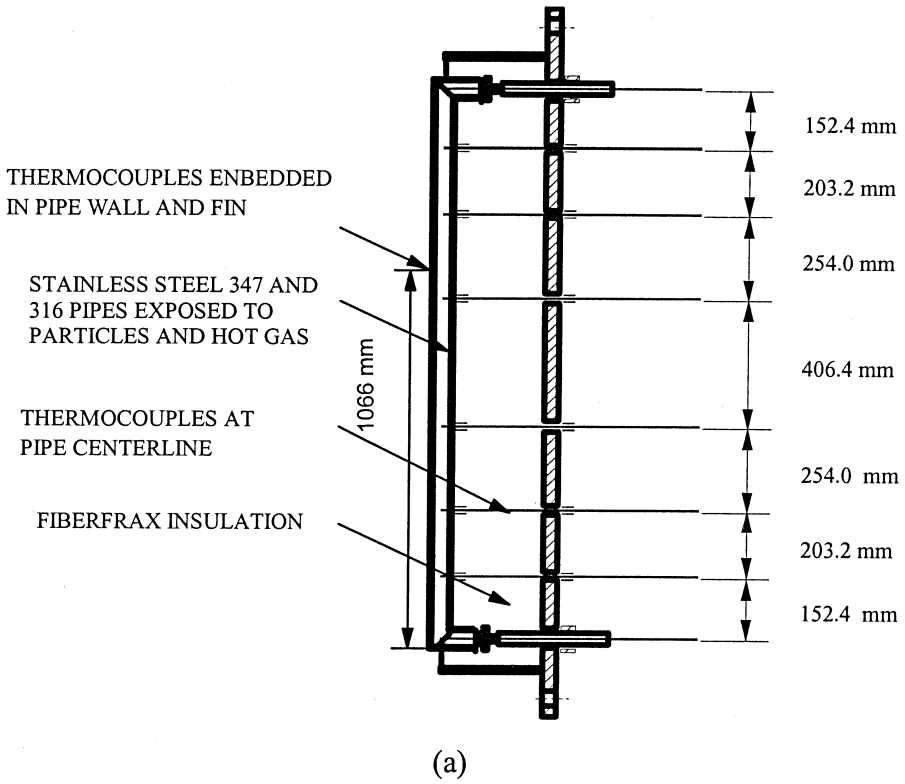

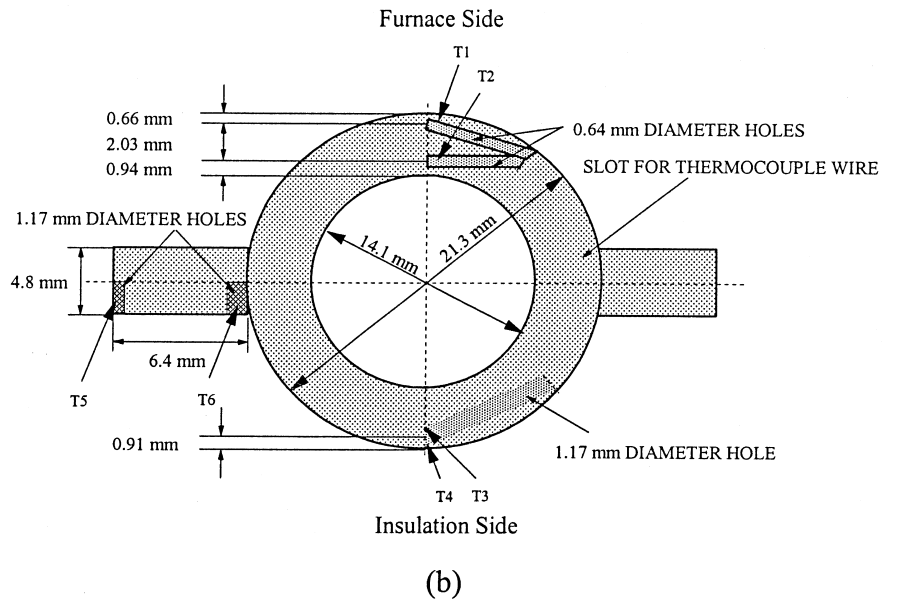

Fig. 1. (a) Schematic diagram of representative section of membrane wall. (b) Positions of thermocouples embedded in pipe wall and fin 560 mm below top of membrane wall assembly.

Table 1
Particle size analyses and fluidization properties for Ottawa silica sand

Size range (μm)		Weight fraction (wt%)	
<	⩾	Before run	After run
1000	500	6.7	1.0
500	355	26.1	20.4
355	250	44.7	41.9
250	180	24.7	28.3
180	125	3.6	5.3
125	Pan	0.2	3.1
Sauter mean diameter (μm)		286	264
Sand density (kg/m^3)[a]		2596	2409
Minimum fluidization velocity at 20°C and 101.3 kPa		0.080	0.064

[a] Measured using water displacement method.

T1–T6 in Fig. 1. The bottom of the membrane surface was 4.37 m above the primary air distributor. Other experimental details are provided by Luan [11].

3. Experimental results and discussion

Suspension axial temperature profiles near the centerline of the riser were nearly uniform over the interval where the membrane wall was located [11]. However, significant lateral gradients of temperature can occur normal to the wall close to cooling surfaces in CFB furnaces [4,12,13]. As indicated above, thermal boundary layers develop along the transfer surface. To estimate and predict suspension-to-surface heat transfer coefficients under non-isothermal conditions, an expression is needed for the temperature profile close to the surface.

The local suspension temperature was measured with a K-type thermocouple, 1 mm in diameter, inserted into the riser from a port opposite the membrane wall, 5.44 m above the air distributor [11]. This thermocouple was shielded by two concentric stainless steel pipes, with the end of the pipe facing the combustor blocked to avoid radiation to the membrane wall. A conical hole with top and bottom diameters of 10 and 6 mm, respectively, was drilled at the blocked end with its axis vertical, and the thermocouple head was fixed at the center of the hole. The thermocouple was tested using an ice–water mixture and boiling water revealing that the accuracy was better than ± 0.5°C for the temperature range of 0–100°C. A similar accuracy probably pertains to the 800–900°C temperature range since the electromotive force for nickel–chromium/nickel–aluminum thermocouples increases linearly with temperature and its thermopower remains practically constant over a wide temperature band, e.g. 40.95 μV/°C in the 0–100°C range and 40.48 μV/°C in the 800–900°C range [14].

The experiments were performed at several bulk suspension temperatures. The results indicated that there were substantial temperature gradients close to the wall for the conditions studied. The lateral temperature profiles were uniform across the cross-section of the riser core, while there was a thermal boundary layer in the annular region. Local temperature gradients have also been observed in commercial CFBC risers [1,8,12,13,15].

Measured temperature profiles in the vicinity of the pipe crest from this study are compared with data reported by others in Fig. 2 (see also Table 2). There are steep temperature gradients close to the water-cooled surface, with temperature increasing with increasing distance from the fin and pipe crest. Our results are qualitatively consistent with earlier observations. Fig. 2 also indicates an effect of scale on the temperature profile for similar operating conditions, with our riser being smaller than those used in the other studies. In our case, the thermal boundary layer was about 15–20 mm thick at the location where measurements were made, whereas the corresponding thickness in commercial CFB boilers is typically 100–200 mm [13,16].

The heat fluxes from the suspension to the pipe and fin are important in determining the membrane wall efficiency. Estimation of these fluxes requires knowledge of the temperature distributions in the pipe and fin. The measured temperatures in the pipe and fin, as well as the crest and fin temperature differences, are plotted for two bulk temperatures in Fig. 3.

The temperature at the center of the fin (T_5) is seen to be higher than near the crest of the pipe wall (T_1). The similarity of T_1 and T_6 indicates that the heat flux through the pipe wall is essentially one-dimensional in the radial direction over the exposed portion of the pipe. The fact that T_3 and T_4 are so similar confirms that there is little heat loss through the insulation. The temperature difference ($T_1 - T_2$) is typically 10–18°C, while ($T_5 - T_6$) is typically 21–26°C for a suspension density of 40 kg/m^3 at bulk suspension temperatures of 700–800°C. Note that the temperature differences increase with increasing suspension density, indicating that more heat is being transferred from the suspension to the membrane walls, i.e., there is less thermal resistance on the suspension side. Temperatures along the periphery of a pipe and fin measured by Andersson and Leckner [1] showed that the temperature difference between the pipe crest and the junction of the pipe and the fin was about 10°C, while the difference between the junction of the fin and the center of the fin was about 5°C at similar thermocouple locations for a pipe

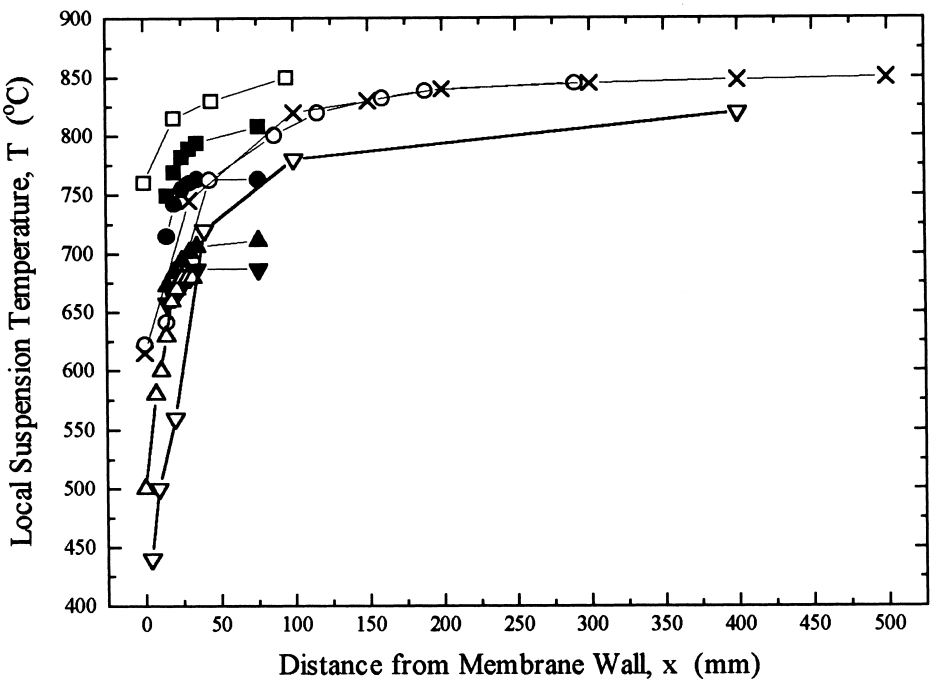

Fig. 2. Lateral suspension temperature profiles near membrane walls, measured from fin. For symbols and conditions, see Table 2.

of diameter 60.3 mm and fin of width 8.8 mm. However, the exact locations of their thermocouples were not identified. The differences between the $(T_1 - T_6)$ and $(T_5 - T_6)$ results of Andersson and Leckner [1] and those of this study are no doubt caused by their larger pipe (diameter 60.3 mm compared with 21.3 mm) and narrower fin (8.8 mm compared with 12.7 mm).

Several models have been developed to calculate heat fluxes and temperature profiles in pipe/fin assemblies [1,6,8,9,17,18]. The temperature distributions obtained using these models indicate that radial one-dimensional heat flow gives a good approximation for the exposed portion of the pipe wall. The exposed-pipe-radial, insulated-pipe-tangential, fin-one-dimensional model (model 2) proposed by Bowen et al. [6] is used here to estimate the suspension-to-pipe-and-fin average heat transfer coefficients from measured changes in the cooling water temperature. This model gave excellent accuracy with limited computational effort. The temperatures measured by the embedded thermocouples are also used with the model to estimate local suspension-to-pipe, suspension-to-fin and suspension-to-total-surface heat transfer coefficients. The model is shown schematically in Fig. 4. Heat is transferred from the suspension through two sections

Table 2
Symbols and parameters for temperature profiles plotted in Fig. 2

Symbol in Fig. 2	Reference	Riser cross-section (m^2)	T_b (°C)	d_p (μm)	ρ_{susp} (kg/m^3)	P/S	U_g (m/s)	z/H
▽	Leckner and Andersson [1]	1.7 × 1.7	850	260	N/A[a]	3.35	4.0	0.86
△	Jestin et al. [8]	8.6 × 11	725	260	N/A	N/A	N/A	N/A
□	Couturier et al. [13]	3.96 × 3.96	880	N/A	N/A	N/A	N/A	N/A
○	Golriz [14]	1.7 × 1.7	845	290	3–70	2.33	2.6–6.6	0.81
×	Werdermann and Werther [16]	5.13 × 5.13	850	215	5–7	N/A	N/A	0.74
■	This work	0.152 × 0.152	808	286	45–72	2.0	8.0	0.73
●	This work	0.152 × 0.152	763	286	45–72	2.0	8.0	0.73
▲	This work	0.152 × 0.152	711	286	45–72	2.0	8.0	0.73
▼	This work	0.152 × 0.152	687	286	45–72	2.0	8.0	0.73

[a] N/A: not available.

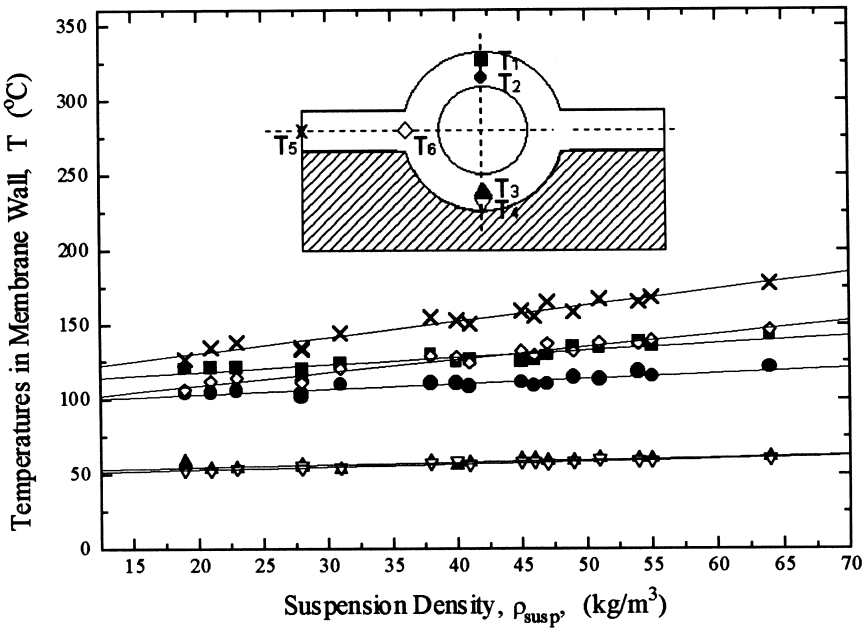

(a)

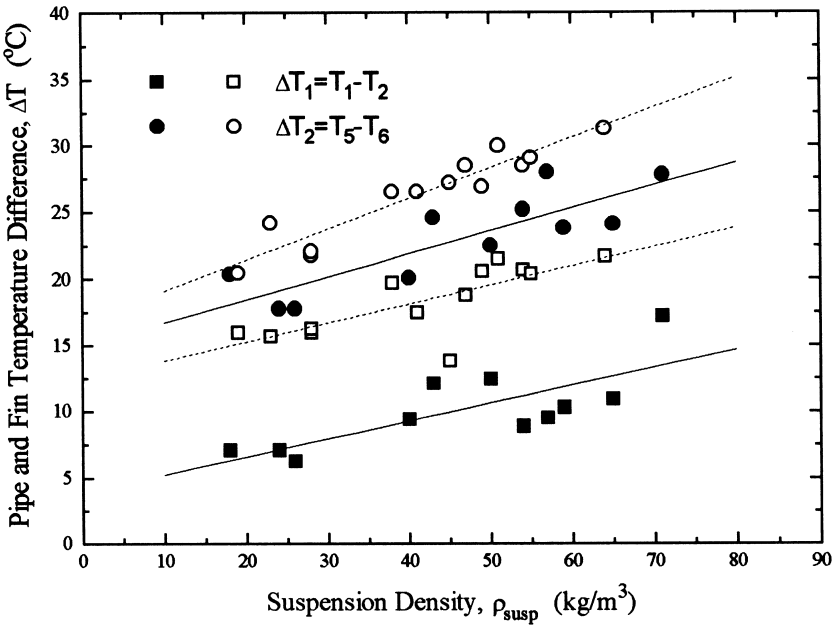

(b)

Fig. 3. (a) Temperature distribution in pipe and fin versus suspension density. $T_b = 804 \pm 5°C$. (b) Pipe and fin temperature difference distributions measured by embedded thermocouples. Open symbols: $T_b = 804 \pm 5°C$; solid symbols: $T_b = 706 \pm 4°C$. Dotted lines: best linear fits for $T_b = 804 \pm 5°C$; solid lines: best linear fits for $T_b = 706 \pm 4°C$. Operating conditions: $d_p = 286$ μm, $P/S = 2.0$, $U_g = 8.0$–8.5 m/s, $z = 5.44$ m.

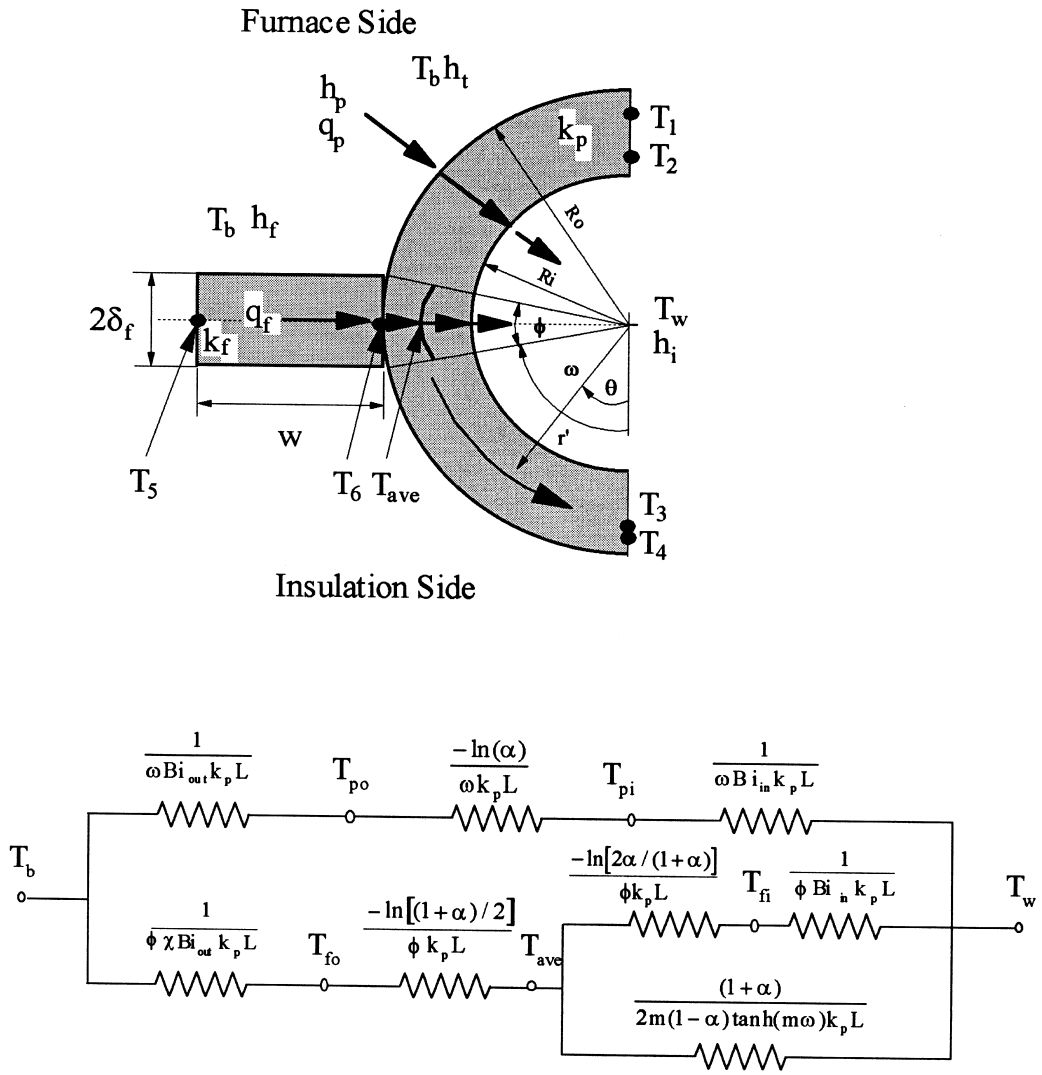

Fig. 4. Schematic of exposed-pipe-radial, insulated-pipe-tangential, fin-one-dimensional heat transfer model of Bowen et al. [6] and electrical circuit analogue. Position of thermocouples used in the experiments are indicated by T_1–T_6.

in parallel: the exposed pipe section and the fin section. The thermal resistance for the pipe section must account for convection and radiation from the suspension to the outer surface of the pipe, radial conduction through the pipe and convective transfer to the cooling water inside the pipe. The thermal resistance in the fin section considers one-dimensional conduction along the fin in addition to convective and radiative transfer to one side of the fin. From the fin/pipe junction, heat flows to the cooling water by two parallel paths: by radial conduction through the abutted sector of the pipe, and by tangential conduction through the insulated portion of the pipe. These paths are indicated by arrows in Fig. 4. An electric circuit analogue [6] then leads to:

$$Q_t = 2\left[k_p L\left(T_b - \frac{T_{w,out} + T_{w,in}}{2}\right)\right] \times \left[\frac{\phi}{C_2 + (1/\chi Bi_{out})} + \frac{\omega}{C_3 + (1/Bi_{out})}\right] \quad (1)$$

where Q_t is the total heat transfer rate ($= M_{cw} c_{p,cw}(T_{w,out} - T_{w,in})$) and:

$$C_1 = \frac{Bi_{in}}{1 - Bi_{in}\ln[2\alpha/(1+\alpha)]} + \frac{2(1-\alpha)m\tanh(m\omega)}{(1+\alpha)\phi} \quad (2a)$$

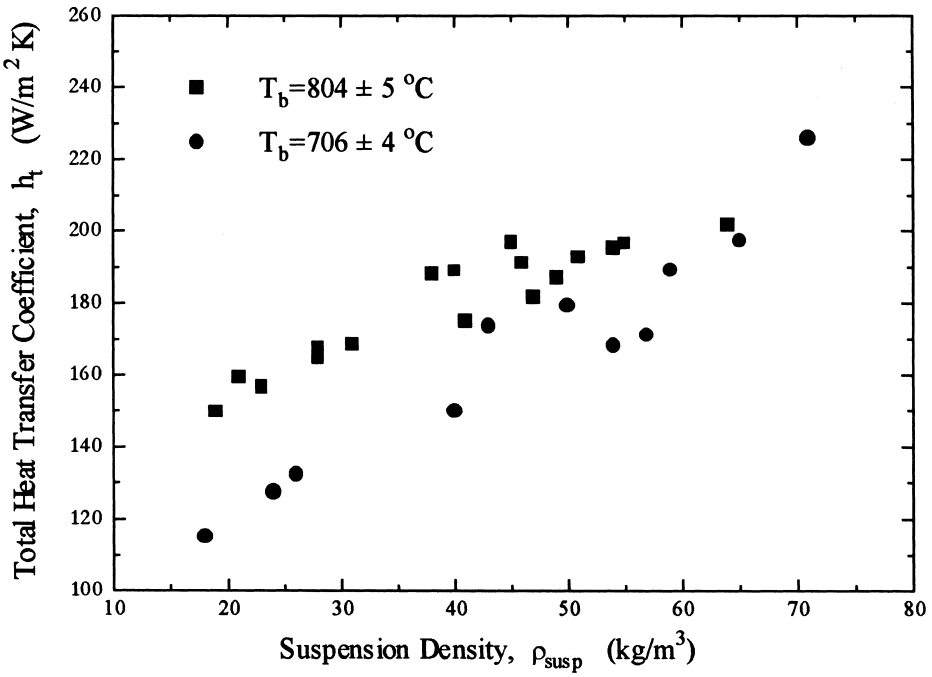

Fig. 5. Effect of suspension density on suspension-to-membrane-wall heat transfer coefficient determined from local temperature measurements for different suspension temperatures. $d_p = 286$ μm, $U_g = 8.0$–8.5 m/s, $P/S = 2.0$.

$$C_2 = \frac{1}{C_1} - \ln\left(\frac{1+\alpha}{2}\right) \tag{2b}$$

$$C_3 = \frac{1}{Bi_{in}} - \ln\alpha \tag{2c}$$

$$m = \left[\frac{Bi_{in}(1+\alpha)}{2(1-\alpha)}\right]^{1/2} \tag{2d}$$

$$\chi = \left(\frac{\zeta}{2\beta Bi_{out}}\right)^{1/2} \tanh\left[\left(\frac{Bi_{out}}{2\beta\zeta}\right)^{1/2}\gamma\right] \tag{2e}$$

with

$$Bi_{in} = \frac{h_i R_i}{k_p};\quad Bi_{out} = \frac{h_t R_o}{k_p};\quad \alpha = \frac{R_i}{R_o};\quad \beta = \frac{\delta_f}{R_o};$$

$$\gamma = \frac{w}{R_o};\quad \zeta = \frac{k_f}{k_p};\quad \phi = 2\sin^{-1}(\beta);\quad \omega = \frac{\pi-\phi}{2}.$$

We estimate h_i from the correlation of Sleicher and Rouse [19] as in Ref. [20]; k_p and k_f are evaluated, respectively, at the average pipe and average fin temperatures measured by the embedded thermocouples. Since Eq. (1) is implicit in h_t, the average outside heat transfer coefficient for each experimental Q_t value was determined numerically using the Newton–Raphson method.

As shown in Fig. 5, the average suspension-to-membrane wall heat transfer coefficients obtained using Eq. (1) varied between 140 and 260 W/m^2 K for the conditions investigated, increasing with both increasing suspension density and increasing bulk suspension temperature.

The total suspension-to-exposed-surface heat transfer rate is equal to the sum of the heat transfer rates through the pipe and the fin. The heat transfer rate for the pipe, Q_p, is given by

$$Q_p = \frac{T_1 - T_2}{\ln(r_1/r_2)/(2\omega L k_p)} \tag{3}$$

where r_1 and r_2 are the radial locations of thermocouples T_1 and T_2, respectively, and L is the length of the pipe. The suspension-to-pipe heat transfer coefficient, based on the exposed pipe area, can then be determined from

$$h_p = \frac{Q_p}{2\omega R_o L(T_b - T_{po})} \tag{4}$$

where T_{po} is the temperature of the outside surface of the pipe, determined by logarithmic extrapolation of T_1 and T_2 to $r = R_o$.

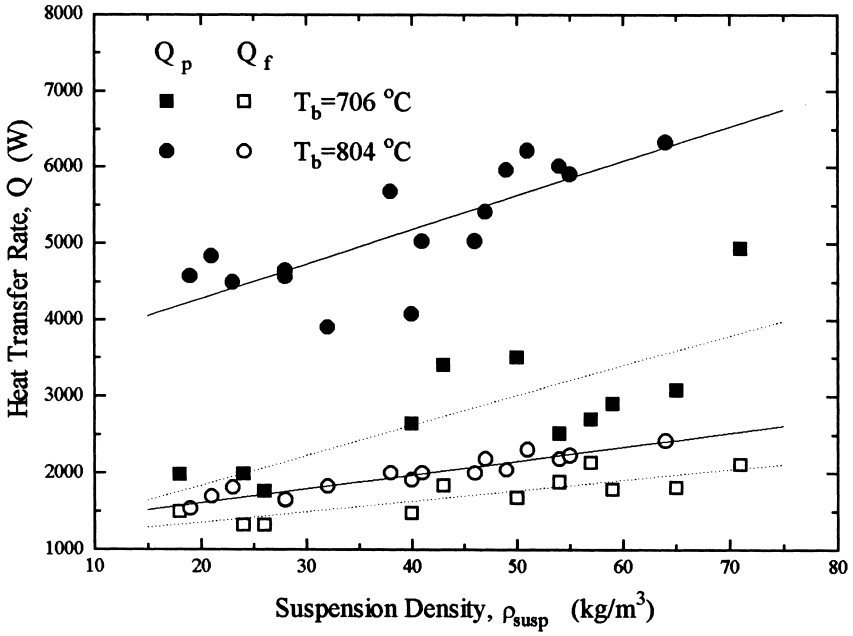

Fig. 6. Suspension-to-pipe and suspension-to-fin heat transfer rates versus suspension density. $d_p = 286$ μm, $P/S = 2.0$, $U_g = 8.0 - -8.5$ m/s, $z = 5.44$ m. Q_p and Q_f are evaluated using $(T_1 - T_2)$ and $(T_5 - T_6)$, respectively. The lines are best linear fits.

With the assumptions that: (1) conduction through the fin is essentially one-dimensional, (2) the fin is adiabatic at the plane equidistant between the two pipes, and (3) the non-exposed side of the fin assembly is well insulated, the suspension-to-fin heat transfer rate is given by

$$Q_f = L\sqrt{2\delta_f k_f h_f}(T_b - T_6)\tanh(m\omega) \tag{5}$$

where the suspension-to-fin heat transfer coefficient is:

$$h_f = 2\delta_f k_f m^2 \tag{6}$$

and m can be determined from the measured temperatures, T_b, T_5 and T_6 as:

$$m = \frac{1}{\omega}\cosh^{-1}\left(\frac{T_b - T_5}{T_b - T_6}\right) \tag{7}$$

The total uniform suspension-to-total-surface heat transfer rate and coefficient based on the exposed area of the pipe and fin can now be obtained from

$$Q_t = Q_p + Q_f \tag{8}$$

and

$$h_t = \frac{Q_p + Q_f}{(A_p + A_f)(T_b - T_{surf})} \tag{9}$$

where A_p $(= 2\omega R_o L)$ and A_f $(= 2wL)$ are the exposed pipe and fin areas, respectively. T_{surf} is the weighted-average exposed surface temperature of the pipe and fin estimated as $T_{surf} = [A_f(T_5 + T_6)/2 + A_p T_{po}]/[A_p + A_f]$.

The suspension-to-pipe and suspension-to-fin heat transfer rates determined in this manner are plotted against suspension density in Fig. 6. The heat transfer rates to the pipe and fin differ significantly. Suspension-to-pipe transfer is enhanced by increasing either the suspension density or the suspension temperature; both parameters have less impact on the suspension-to-fin heat transfer rate. The suspension-to-fin heat transfer accounts for about 32–44% of the total heat transfer rate at 706°C, and about 25–32% at 804°C.

Visual observations [1,21] of particle flow patterns near membrane walls have shown that falling solids tend to gather in the troughs along the fins between adjacent pipes. When the suspension density is high enough that the emulsion boundary layer covers both the pipe and fin, this layer is thinner along the pipe crest than along the fin. The particle concentration is also lower at the crest than in the trough [2,20,22]. Hence, increasing the suspension density has a greater impact on transfer to the pipe than to the fin. In addition, the particle temperature along the fin falls quickly with length due to the reduced exchange of solids with the bulk, decreasing the heat transfer driving force and resulting in decreased transfer to the fin.

Fig. 7 shows that h_t, h_p and h_f increase with increasing suspension density; $h_p > h_f$ for 804°C, while $h_p <$

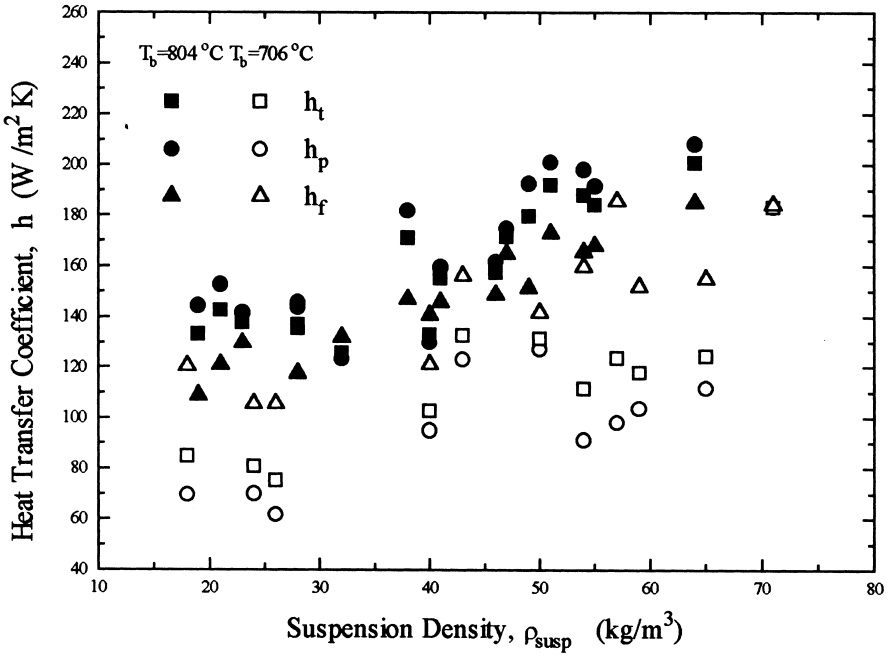

Fig. 7. Suspension-to-pipe, suspension-to-fin and total suspension-to-membrane-wall heat transfer coefficients versus suspension density. $d_p = 286$ μm, $P/S = 2.0$, $U_g = 8.0$–8.5 m/s, $z = 5.44$ m. Solid symbols: $T_b = 804 \pm 5$°C; open symbols: $T_b = 706 \pm 4$°C.

h_f for 706°C. This suggests that the fin becomes less efficient than the crest of the pipe in extracting heat as radiation becomes more important in this relatively small riser where the wall layer is thin and where only one face is cooled. Given the lower transfer to the fins for long surfaces and the conductive resistance along the fins, their widths should be limited in order to increase the efficiency of membrane walls when thermal radiation is significant. However, the fin width should be at least $20d_p$ to ensure that particles can circulate freely without bridging in the troughs [23]. The h_p at 804°C is higher than that at 706°C because of the augmented radiative component and higher gas conductivity.

The total suspension-to-membrane-wall heat transfer rates determined in a second manner from the measured inlet and outlet water temperatures (Eq. (1)), are compared with the values estimated from the embedded thermocouple readings (Eq. (8)) in Fig. 8, assuming lengthwise uniformity. The total heat transfer based on the inlet and outlet water temperatures is about 8.5% higher on average than the rate based on the embedded thermocouples at 804°C, and 28.0% higher at 706°C. These discrepancies are probably due to lengthwise variations along the assembly and to the uncertainty of the local temperature values, since it is difficult to precisely determine the thermocouple positions. Error analyses indicate that the heat flux determined from temperatures in the pipe and fin is sensitive to the distance between adjacent thermocouples. A 0.25 mm offset from the assumed positions could cause deviations from −20 to +33% in the heat flux from the pipe crest and −3.7 to +4.2% for the fin.

The temperature distribution along the insulated portion of the pipe wall is given [6] by

$$T(\theta) = T_w - (T_w - T_{ave})\frac{\cosh(m\theta)}{\cosh(m\omega)} \tag{10}$$

where T_w is the local cooling water temperature (approximated as $(T_{w,in} + T_{w,out})/2$), and T_{ave} is the temperature at the center of the pipe wall adjacent to the fin. T_{ave} can be calculated from T_6, the temperature at the pipe-fin junction, and Q_f, the fin heat transfer rate from Eq. (5), using

$$T_{ave} = T_6 - Q_f\frac{\ln[2/(1+\alpha)]}{\phi k_p L} \tag{11}$$

The temperatures at $\theta = 0$, estimated using Eq. (10), are compared with the measured temperatures $T_m = (T_3 + T_4)/2$ (see Fig. 1) in Fig. 9. The measured and calculated temperatures are seen to agree well with each other, with the average deviation between the predicted and measured temperatures being 3.4% for this study.

The ratio of the heat transfer rate through the insu-

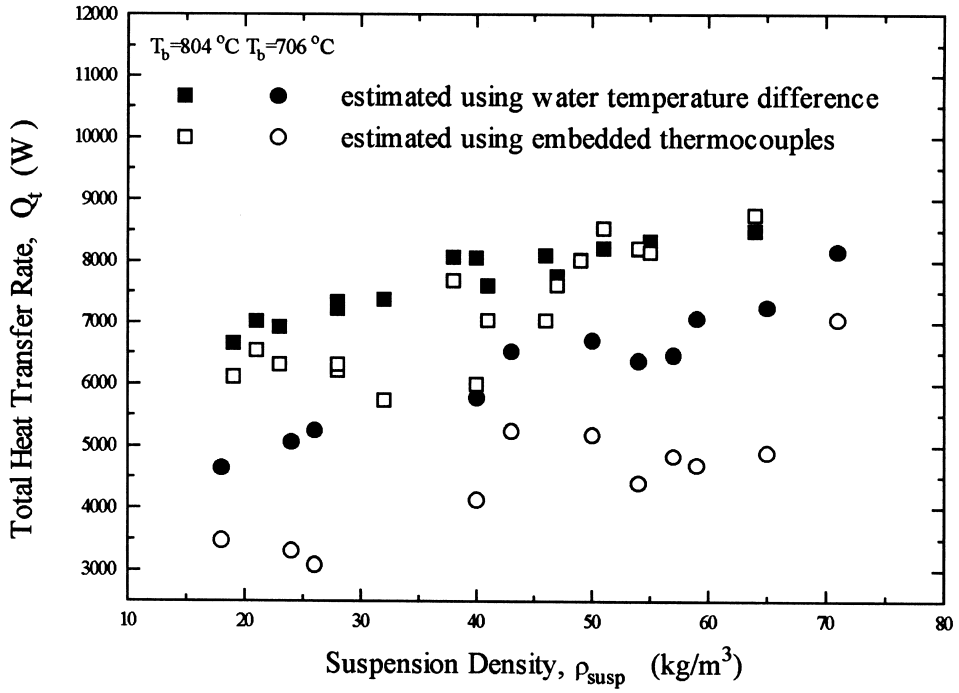

Fig. 8. Suspension-to-membrane-wall heat transfer rate from overall heat balance method versus suspension density. $d_p = 286$ μm, $P/S = 2.0$, $U_g = 8.0$–8.5 m/s, $z = 5.44$ m.

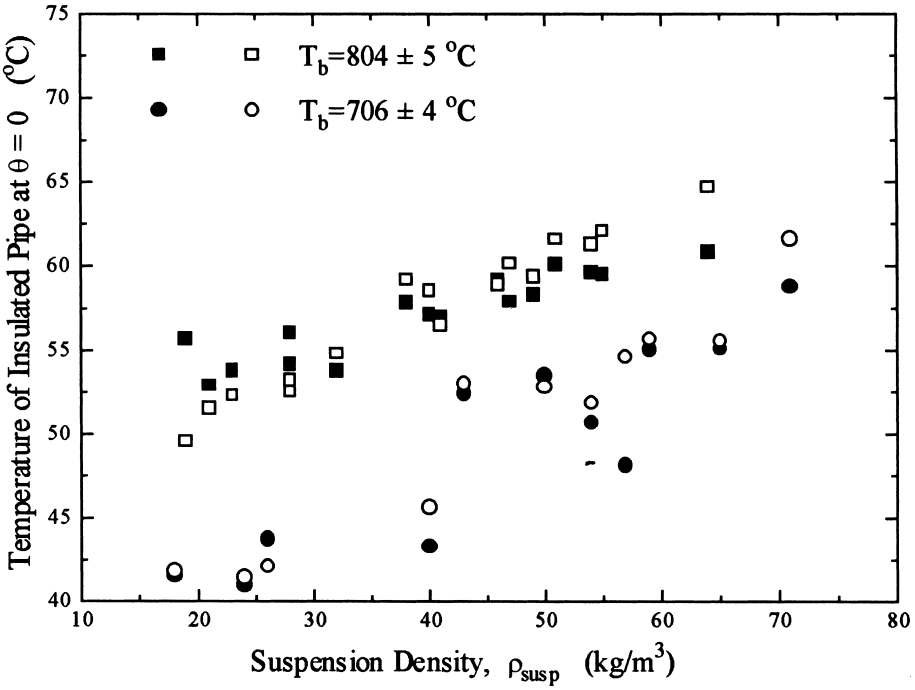

Fig. 9. Temperatures of insulated pipe at $\theta = 0$ versus suspension density. Solid symbols: measured temperatures; open symbols: temperatures predicted by model 2 of Bowen et al. [6].

lated portion of the pipe ($0 < \theta < \omega$) to the heat transfer rate through the fin can be estimated from

$$\frac{Q_{\text{ins}}}{Q_{\text{f}}} = \frac{1}{\dfrac{1}{\dfrac{1}{\phi Bi_{\text{in}}} + \dfrac{\ln[(1+\alpha)/2\alpha]}{\phi}} + \dfrac{1}{\dfrac{(1+\alpha)}{2m(1-\alpha)\tanh(m\omega)}}} \Bigg/ \frac{(1+\alpha)}{2m(1-\alpha)\tanh(m\omega)} \tag{12}$$

Under the conditions of this study, about 64% of the heat flow from the fin is transferred through the insulated portion of the pipe to the cooling water, with the remainder dissipated by the section of pipe immediately abutting the fin ($\omega < \theta < \omega + \phi$). In this paper, we have not separately considered radiation and convection. These components are treated separately and compared with appropriate models elsewhere [24].

4. Conclusions

1. Temperatures measured by thermocouples embedded in a pipe and fin of a membrane wall assembly indicate that the heat flows through the pipe and fin are nearly one-dimensional. Model 2 of Bowen et al. [6] can, therefore, be used to estimate heat transfer coefficients.
2. Suspension-to-membrane-wall heat transfer coefficients increase with suspension density as in previous work. The bulk suspension temperature also has a major influence on the total heat transfer coefficient, primarily due to radiation.
3. The thickness of the thermal boundary layer in the pilot combustor is about 15–20 mm for the conditions studied.
4. The suspension-to-pipe heat transfer coefficient is higher than the suspension-to-fin heat transfer coefficient, indicating that the fin is not as efficient as the exposed pipe surface for long membrane walls. About one-third of the transferred heat passes through the fin, and approximately 64% of that is transferred to the coolant via the insulated portion of the pipe.

Acknowledgements

Financial support from both Energy, Mines and Resources Canada (now Natural Resources Canada) and the Natural Sciences and Engineering Research Council of Canada is gratefully acknowledged.

References

[1] B.-Å. Andersson, B. Leckner, Experimental methods of estimating heat transfer in circulating fluidized bed boilers, Int. J. Heat Mass Transfer 35 (1992) 3353–3362.
[2] C. Lockhart, J. Zhu, C.M.H. Brereton, C.J. Lim, J.R. Grace, Local heat transfer, solids concentration and erosion around membrane tubes in a cold model circulating fluidized bed, Int. J. Heat Mass Transfer 38 (1995) 2403–2410.
[3] R.L. Wu, C.J. Lim, J. Chaouki, J.R. Grace, Heat transfer from a circulating fluidized bed to membrane waterwall surfaces, AIChE J. 33 (1987) 1888–1893.
[4] B. Leckner, B.-Å. Andersson, Characteristic features of heat transfer in circulating fluidized bed boiler, Powder Technology 70 (1992) 303–314.
[5] G. Flamant, N. Fatah, G. Olalde, D. Hernandez, Temperature distribution near a heat exchanger wall immersed in high-temperature packed and fluidized beds, J. Heat Transfer 114 (1992) 50–55.
[6] B.D. Bowen, M. Fournier, J.R. Grace, Heat transfer in membrane waterwalls, Int. J. Heat Mass Transfer 34 (1991) 1043–1057.
[7] L. Jestin, C. Chabert, G. Flamant, P. Meyer, In-situ measurement of particle concentration, temperature distribution and heat flux in the vicinity of a wall in a CFB, in: P. Basu, M. Horio, M. Hasatani (Eds.), Circulating Fluidized Bed Technology III, Pergamon Press, Oxford, 1990, pp. 247–251.
[8] L. Jestin, P. Meyer, G. Schmitt, J.X. Morin, Heat transfer in a 125 MWe CFB boiler, in: O.E. Potter, D.J. Nicklin (Eds.), Fluidization VII, Engineering Foundation, New York, 1992, pp. 849–856.
[9] J. Taler, A method of determining local heat flux in boiler furnaces, Int. J. Heat Mass Transfer 35 (1992) 1625–1634.
[10] W. Luan, C.J. Lim, C.M.H. Brereton, B.D. Bowen, J.R. Grace, Measurement of radiative heat transfer in a circulating fluidized bed combustor, in: F.D.S. Preto (Ed.), Proc. Fourteenth Intl. Fluidized Bed Combustion Conf., vol. 2, ASME, New York, 1997, pp. 879–884.
[11] W. Luan, Radiative and total heat transfer in circulating fluidized beds, Ph.D. dissertation, University of British Columbia, Vancouver, Canada, 1997.
[12] M.F. Couturier, F. Steward, S. Poolpol, Experimental determination of heat transfer coefficients in a 72 MW circulating fluidized bed boiler, in: L. Rubow (Ed.), Proc. Twelfth Intl. Fluidized Bed Combustion Conf., vol. 2, ASME, New York, 1993, pp. 1215–1222.
[13] M.R. Golriz, An experimental correlation for temperature distribution at the membrane wall of CFB boilers, in: K.J. Heinschel (Ed.), Proc. Thirteenth Intl. Fluidized Bed Combustion Conf., vol. 1, ASME, New York, 1995, pp. 499–505.
[14] T.J. Quinn, Temperature, Academic Press, London, 1990.
[15] C.C. Werdermann, J. Werther, Heat transfer in large-scale circulating fluidized bed combustors of different sizes, in: A.A. Avidan (Ed.), Circulating Fluidized Bed Technology IV, AIChE, New York, 1994, pp. 428–435.

[16] K.E. Wirth, Wall-to-suspension heat transfer in circulating fluidized beds, in: K.J. Heinschel (Ed.), Proc. Thirteenth Intl. Fluidized Bed Combustion Conf., vol. 1, ASME, New York, 1995, pp. 473–486.
[17] D.R. Raymond, J.W. Rauscher, Heat transfer determination in boiler waterwall tubes using fin temperature measurements, Tappi Journal 67 (7) (1984) 76–79.
[18] D. Montat, A. Arhaliass, G. Schmitt, O. Piedfer, P. Snabre, L. Jestin, Heat transfer measurement and analysis in a 125 MWe circulating fluidized bed boiler, in: L. Rubow (Ed.), Proc. Twelfth Intl. Fluidized Bed Combustion Conf., vol. 2, ASME, New York, 1993, pp. 1207–1213.
[19] C.A. Sleicher, M.W. Rouse, A convenient correlation for heat transfer to constant and variable property fluids in turbulent pipe flow, Int. J. Heat Mass Transfer 18 (1975) 677–683.
[20] R.L. Wu, Heat transfer in circulating fluidized beds, Ph.D. dissertation, University of British Columbia, Vancouver, Canada, 1989.
[21] R.L. Wu, C.J. Lim, J.R. Grace, C.M.H. Brereton, Instantaneous local heat transfer and hydrodynamics in a circulating fluidized bed, Int. J. Heat Mass Transfer 34 (1991) 2019–2027.
[22] B. Leckner, Heat transfer in circulating fluidized bed boilers, in: P. Basu, M. Horio, M. Hasatani (Eds.), Circulating Fluidized Bed Technology III, Pergamon Press, Toronto, 1990, pp. 27–37.
[23] J.R. Grace, Fluidized-bed hydrodynamics, in: G. Hetsroni (Ed.), Handbook of Multiphase Systems, Hemisphere, Washington, 1982.
[24] W. Luan, C.J. Lim, C.M.H. Brereton, B.D. Bowen, J.R. Grace, Experimental and theoretical study of total and radiative heat transfer in circulating fluidized beds, Chem. Eng. Sci. 54 (1999) 3749–3764.